nature immunology

Complementarity and redundancy of IL-22-producing innate lymphoid cells

Lucille C Rankin[1,2,15,16], Mathilde J H Girard-Madoux[3,16], Cyril Seillet[1,2], Lisa A Mielke[1,2], Yann Kerdiles[3], Aurore Fenis[3], Elisabeth Wieduwild[3], Tracy Putoczki[1,2], Stanislas Mondot[4], Olivier Lantz[5], Dieter Demon[6,7], Anthony T Papenfuss[1,2], Gordon K Smyth[1,2,8], Mohamed Lamkanfi[6,7], Sebastian Carotta[1,2,9], Jean-Christophe Renauld[10], Wei Shi[1,2,11], Sabrina Carpentier[12], Tim Soos[13], Christopher Arendt[13], Sophie Ugolini[3], Nicholas D Huntington[1,2], Gabrielle T Belz[1,2,17] & Eric Vivier[3,14,17]

Intestinal T cells and group 3 innate lymphoid cells (ILC3 cells) control the composition of the microbiota and gut immune responses. Within the gut, ILC3 subsets coexist that either express or lack the natural cytoxicity receptor (NCR) NKp46. We identified here the transcriptional signature associated with the transcription factor T-bet–dependent differentiation of NCR$^-$ ILC3 cells into NCR$^+$ ILC3 cells. Contrary to the prevailing view, we found by conditional deletion of the key ILC3 genes *Stat3*, *Il22*, *Tbx21* and *Mcl1* that NCR$^+$ ILC3 cells were redundant for the control of mouse colonic infection with *Citrobacter rodentium* in the presence of T cells. However, NCR$^+$ ILC3 cells were essential for cecal homeostasis. Our data show that interplay between intestinal ILC3 cells and adaptive lymphocytes results in robust complementary failsafe mechanisms that ensure gut homeostasis.

Dysregulation of intestinal barrier function disrupts gut microbiota and results in inflammation, diarrhea and chronic disease. Mucosal immunity is essential for control of the composition of gut commensal flora and maintenance of health in the face of continual exposure to potentially pathogenic bacteria in the gastrointestinal tract. Interleukin 22 (IL-22) has a crucial role in this immunological control of gut commensal and pathogenic bacteria and is secreted by a heterogeneous population of lymphocytes that express the nuclear hormone receptor and transcription factor RORγt (encoded by *Rorc*)[1], including subsets of helper T cells (T_H17 and T_H22) and group 3 innate lymphoid cells (ILC3 cells)[2–7].

ILC3 cells are a heterogeneous population of innate lymphoid cells (ILCs) that are particularly abundant at mucosal sites. They can be divided into three main subsets on the basis of their role during embryogenesis and their cell-surface expression of the natural cytoxicity receptor (NCR) NKp46 (called 'NCR$^+$' or 'NCR$^-$' cells here). NCR$^-$ ILC3 cells are lymphoid tissue–inducer cells that were originally identified in the fetus and are required for the development of lymph nodes and Peyer's patches[8]. Lymphoid tissue–inducer cells do not require expression of the transcription factor PLZF[9] and can be categorized as CD4$^-$ or CD4$^+$ cells. Another subset of NCR$^-$ ILC3 cells requires PLZF and gives rise to NCR$^+$ ILC3 cells in a manner dependent on the transcription factor T-bet and the Notch family of receptors[10,11]. NCR$^-$ ILC3 cells can promote colitis in a model of inflammatory bowel disease[12]. In contrast, NCR$^+$ ILC3 cells are essential for regulation of the balance between commensal bacteria and pathogenic bacteria through their IL-23-driven production of IL-22, particularly during infection with *Citrobacter rodentium*[13,14]. *C. rodentium* is a Gram-negative mouse-restricted pathogenic bacterium that can be used as a model of the human enteric pathogens enteropathogenic *Escherichia coli* and enterohemorrhagic *E. coli*. It colonizes the intestinal mucosa, which leads to the formation of attaching and effacing lesions that result from the effacement of the brush-border microvilli. IL-22 is essential for the control of infection with *C. rodentium*, as it stimulates the secretion of antimicrobial peptides and protects epithelial function[15]. As a consequence, mice that lack this cytokine rapidly succumb to the disease[16]. NCR$^+$ ILC3 cells have a critical role in protection against *C. rodentium* in mice globally deficient in genes also expressed in B cells or T cells, such as *Rag2*, *Tbx21* or *Cxcr6* (refs. 11,13,14,17). However, these mouse models have profound or partial immunodeficiency, which confounds interpretation of findings obtained with these models, as well as delineation of the

[1]The Walter and Eliza Hall Institute of Medical Research, and Department of Medical Biology, University of Melbourne, Parkville, Australia. [2]Department of Medical Biology, University of Melbourne, Parkville, Australia. [3]Centre d'Immunologie de Marseille-Luminy, Université d'Aix-Marseille UM2, Inserm, U1104, CNRS UMR7280, Marseille, France. [4]Labex Milieu Intérieur, Institut Pasteur, Paris, France. [5]Laboratoire d'Immunologie and Inserm U932, Institut Curie, Paris, France. [6]Inflammation Research Center, VIB, Ghent University, Ghent, Belgium. [7]Department of Biochemistry, Ghent University, Ghent, Belgium. [8]Department of Mathematics and Statistics, University of Melbourne, Parkville, Australia. [9]Boehringer-Ingelheim RCV, Vienna, Austria. [10]Ludwig Institute for Cancer Research and Experimental Medicine Unit, Catholic University of Louvain, Brussels, Belgium. [11]Department of Computing and Information Systems, University of Melbourne, Parkville, Australia. [12]MI-mAbs consortium Aix-Marseille University, Centre d'Immunologie de Marseille-Luminy, Marseille, France. [13]Bioinnovation, SANOFI, Boston, Massachusetts, USA. [14]Immunologie, Hôpital de la Conception, Assistance Publique–Hôpitaux de Marseille, Marseille, France. [15]Present address: Weill Cornell Medical College, Cornell University, New York, New York, USA. [16]These authors contributed equally to this work. [17]These authors jointly directed this work. Correspondence should be addressed to G.T.B. (belz@wehi.edu.au) or E.V. (vivier@ciml.univ-mrs.fr).

Received 15 October; accepted 23 October; published online 30 November 2015; doi:10.1038/ni.3332

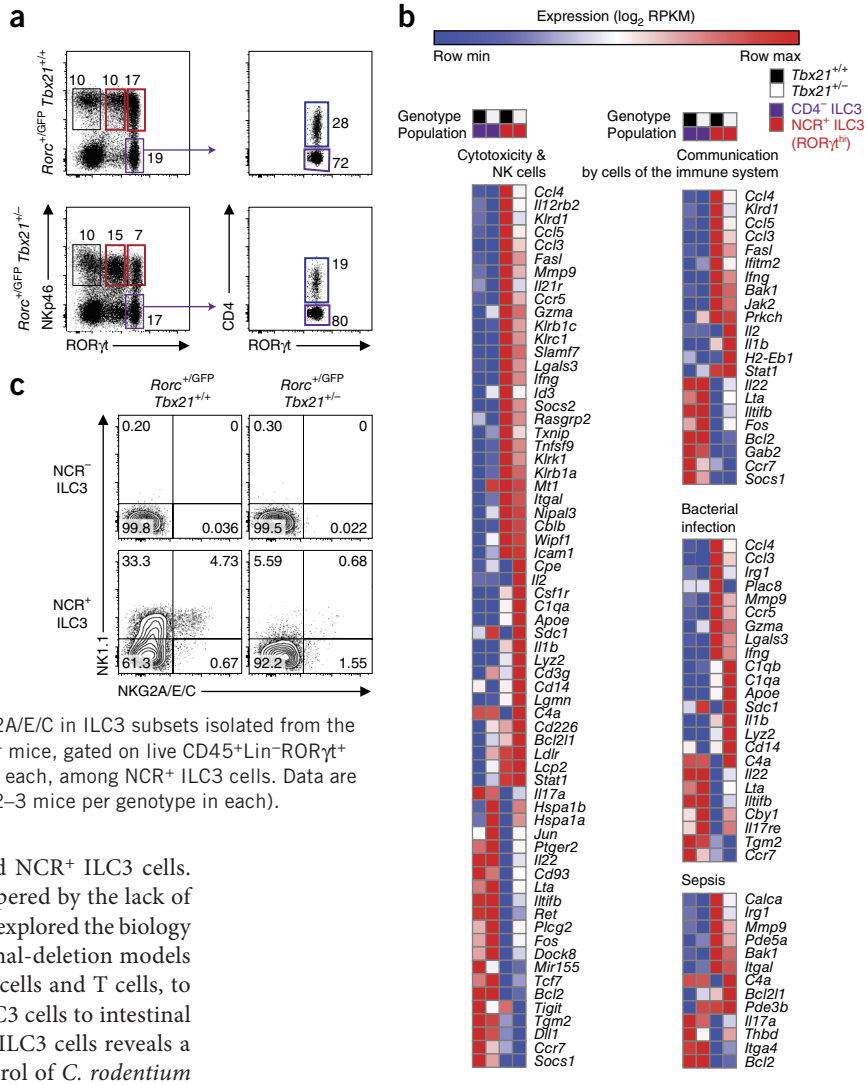

Figure 1 RNA-seq analysis of ILC3 subsets. (**a**) Sorting strategy for ILC3 subsets isolated from the small intestine of *Rorc*$^{+/GFP}$*Tbx21*$^{+/+}$ or *Rorc*$^{+/GFP}$*Tbx21*$^{+/-}$ mice, after gating on live CD45$^+$ Lin$^-$ (CD3$^-$CD19$^-$) cells (left), and segregation of NCR$^-$ ILC3 cells by expression of CD4 and RORγt (right). Numbers adjacent to outlined areas indicate percent NKp46$^+$RORγt$^-$ cells (top left), NKp46$^+$RORγt^{int} ILC3 cells (top middle) or NKp46$^+$RORγt^{hi} ILC3 cells (top right) (NCR$^+$ ILC3 cells), or the NKp46$^-$RORγt$^+$ (NCR$^-$) ILC3 cells sorted further at right (bottom right) (left half), or percent CD4$^+$ NKp46$^-$RORγt$^+$ cells (top) or CD4$^-$ NKp46$^-$RORγt$^+$ cells (bottom) (right half). (**b**) Ingenuity pathway analysis of genes expressed differentially by NCR$^-$ and NCR$^+$ ILC3 cells whose expression was different in *Tbx21*$^{+/+}$ NCR$^+$ ILC3 cells (*Tbx21*$^{+/+}$) than in *Tbx21*$^{+/-}$ NCR$^+$ ILC3 cells (*Tbx21*$^{+/-}$) at steady state (that is, expression affected by the loss of a single copy of the gene encoding T-bet), grouping genes by pathways (above plots) in which their products are involved; expression results are presented as $\log_2$ RPKM values ('reads per kilobase of transcript per million reads'; mean and maximum value for each gene). (**c**) Flow cytometry analyzing NK1.1 and NKG2A/E/C in ILC3 subsets isolated from the intestine of *Rorc*$^{+/GFP}$*Tbx21*$^{+/+}$ and *Rorc*$^{+/GFP}$*Tbx21*$^{+/-}$ mice, gated on live CD45$^+$Lin$^-$RORγt$^+$ cells. Numbers in quadrants indicate percent cells in each, among NCR$^+$ ILC3 cells. Data are representative of two independent experiments (n = 2–3 mice per genotype in each).

selective contributions of NCR$^-$ ILC3 cells and NCR$^+$ ILC3 cells. Overall, analysis of ILC3 biology has been hampered by the lack of models that selectively target these cells. Here we explored the biology of innate producers of IL-22 in mouse conditional-deletion models that targeted NCR$^+$ ILC3 cells but preserved B cells and T cells, to elucidate the specific contributions of NCR$^+$ ILC3 cells to intestinal protection. Our comprehensive analysis of gut ILC3 cells reveals a redundant role for NCR$^+$ ILC3 cells in the control of *C. rodentium* infection in immunocompetent hosts and a selective role for NCR$^+$ ILC3 cells in cecal homeostasis.

RESULTS

Expression profiles of ILC3 subsets

RORγt$^+$ IL-22-producing ILC3 cells have been divided into at least four different subsets, including a T-bet-independent NCR$^-$ ILC3 subset comprising CD4$^+$NKp46$^-$ and CD4$^-$NKp46$^-$ ILC3 cells, and a T-bet-dependent NCR$^+$ ILC3 subset comprising NCR$^+$RORγt^{int} and NCR$^+$RORγt^{hi} ILC3 cells[18,19]. We investigated the relationships among these four ILC3 populations by isolating CD4$^+$NCR$^-$ ILC3 cells (called 'CD4$^+$ ILC3 cells' here), CD4$^-$NCR$^-$ (called 'double-negative (DN) ILC3 cells' here), NCR$^+$RORγt^{int} ILC3 cells and NCR$^+$RORγt^{hi} ILC3 cells from the small intestine of reporter mice with heterozygous expression of sequence encoding green fluorescent protein (GFP) knocked into the *Rorc* locus (*Rorc*$^{+/GFP}$ mice) (**Fig. 1a**) and performing genome-wide transcriptome analysis by high-throughput sequencing technologies for cDNA (RNA-seq). In these NCR$^-$ ILC3 subsets, the transcriptional profiles of the CD4$^+$NCR$^-$ and CD4$^-$NCR$^-$ ILC3 cells were almost identical (**Table 1**), which indicated that they could be considered a single population of NCR$^-$ ILC3 cells. Similarly, NCR$^+$RORγt^{int} and NCR$^+$RORγt^{hi} NCR$^+$ILC3 cells had very similar transcriptional programs (**Table 1**) and differed only in the expression of genes encoding a set of chemokines and chemokine receptors that guide tissue localization, including *Ccl5, Ccl4, Cxcr5* and *Ccr5* (**Supplementary Table 1**). Thus, NCR$^+$RORγt^{int} and NCR$^+$RORγt^{hi} cells were also extremely similar and could be considered a single population of NCR$^+$ ILC3 cells. In contrast, there were robust differences in the transcriptional profiles of NCR$^-$ ILC3 cells and NCR$^+$ ILC3 cells. The expression of genes encoding transcription factors, such as *Idb2*, *Gata3* and *Rorc,* was similar in these subsets, whereas the expression of *Tbx21* and *Prdm1* was upregulated in NCR$^+$ ILC3 cells (**Table 1**). Genes encoding various other transcriptional regulators were also expressed differentially, including *Irf8*, which was upregulated in NCR$^+$ ILC3 cells, and *Batf3* and *Tox2,* which were downregulated in NCR$^+$ ILC3 cells (**Table 1**). Thus, these NCR$^+$ ILC3 cells and NCR$^-$ ILC3 cells were distinct ILC3 subsets with different transcription programs, consistent with a published microarray analysis[20]; this confirmed the validity our RNA-seq approach.

Effect of T-bet on ILC3 cells

T-bet is key to the differentiation of NCR$^-$ ILC3 cells, as NCR$^+$ ILC3 cells are absent from mice deficient in the gene encoding T-bet (*Tbx21*)[10,11,21]; however, the mechanisms by which T-bet affects ILC3 maturation are unclear. We investigated the transcriptional program of ILC3 cells isolated from *Rorc*$^{+/GFP}$*Tbx21*$^{+/-}$ mice, which lack one copy of *Tbx21*. Given that *Rorc*$^{+/GFP}$*Tbx21*$^{+/-}$ mice have a heterogeneous phenotype, we reasoned that the loss of one allele would reveal

Table 1 Genes expressed differentially in ILC3 subsets

		NCR⁻ ILC3 cells		NCR⁺ ILC3 cells	
		CD4⁺	DN	RORγt^{hi}	RORγt^{int}
NCR⁻ ILC3 cells	CD4⁺		19	1,011	744
	DN	20		972	646
NCR⁺ ILC3 cells	RORγt^{hi}	826	751		79
	RORγt^{int}	560	536	84	

Quantification of genes expressed differentially in each comparison of ILC3 populations sorted from *Rorc*$^{+/GFP}$*Tbx21*$^{+/-}$ mice. Rows show genes upregulated (above diagonal) relative to their expression in the population in the corresponding column; columns show genes downregulated (below diagonal) relative to their expression in the population in corresponding row.

differential regulation by T-bet without complete loss of NCR⁺ ILC3 cells, which remained present, albeit at a lower frequency than that in *Rorc*$^{+/GFP}$*Tbx21*$^{+/+}$ mice (**Fig. 1a**). We then performed two types of analyses on the RNA-seq transcriptional profile data set obtained with the following eight ILC3 populations: CD4⁺NCR⁻, CD4⁻NCR⁻ (DN), NCR⁺RORγt^{int} and NCR⁺RORγt^{hi} ILC3 cells from *Tbx21*$^{+/+}$ mice, and the same four subsets from *Tbx21*$^{+/-}$ mice. We first compared the list of genes differentially expressed by NCR⁻ ILC3 cells (CD4⁺ or CD4⁻) and NCR⁺ ILC3 cells (RORγt^{int} or RORγt^{hi}) in *Tbx21*$^{+/+}$ mice with the same list for *Tbx21*$^{+/-}$ mice. In wild-type mice, a total of 674 genes displayed differences in expression by a factor of at least two in NCR⁻ ILC3 cells versus NCR⁺ ILC3 cells; 324 of these genes did not display differential expression between these two cell types in *Tbx21*$^{+/-}$ mice (data not shown). Thus, during the transition from NCR⁻ ILC3 to NCR⁺ ILC3, about 50% of genes were affected by the loss of a single copy of *Tbx21*, which indicated that T-bet guided a substantial component of the NCR⁺ ILC3 developmental program. Second, we compared the gene-expression profiles of ILC3 cells from *Tbx21*$^{+/-}$ mice with those from the corresponding *Tbx21*$^{+/+}$ ILC3 populations. We found no role for T-bet in CD4⁺ or CD4⁻ NKp46⁻ ILC3 cells (data not shown). Therefore, as expected, in NCR⁻ ILC3 populations (CD4⁺ or CD4⁻), very few genes were expressed differentially in *Tbx21*$^{+/+}$ cells relative to their expression in *Tbx21*$^{+/-}$ cells. However, we observed substantial differences in the transcriptional profiles of *Tbx21*$^{+/+}$ NCR⁺ ILC3 cells and *Tbx21*$^{+/-}$ NCR⁺ ILC3 cells (RORγt^{int} or RORγt^{hi}): analysis with a cutoff of a difference in expression at least twofold in *Tbx21*$^{+/+}$ NCR⁺ ILC3 cells versus *Tbx21*$^{+/-}$ NCR⁺ ILC3 cells showed that 72 genes were upregulated and 86 genes were downregulated in *Tbx21*$^{+/+}$ cells (**Supplementary Table 2**). This enabled us to investigate the gene programs specifically regulated by T-bet during generation of the NCR⁺ ILC3 subset. Notably, 70% of the genes found to be downregulated in NCR⁺ ILC3 cells in the absence of T-bet had higher expression in NCR⁺ ILC3 cells than in NCR⁻ ILC3 cells (**Fig. 1b**). Loss of a single allele of T-bet affected genes encoding factors that regulate communication between innate cells and adaptive cells, such as cytokines, chemokines and their receptors, including regulation via IL-2Rα (CD25) and interferon signaling through the Jak-Stat pathway, IL-22, CCL4 and CCL5 (**Fig. 1b**). T-bet also regulated various gene clusters encoding products known to be 'preferentially' associated with effector functions such as cytotoxicity and expressed by natural killer (NK) cells (for example, *Gzme*, *Gzma*, *Ifng* and *Il12rb*) (**Fig. 1b**). These gene clusters also encoded members of the 'killer-cell lectin-like receptor' (KLR) family better known for their inhibitory and activating function in NK cells: *Klri1* (Ly49E1), *Klrd1* (CD94), *Klrb1c* (CD161 or NK1.1) and *Klrc2* (NKG2C) (**Fig. 1b**). Consistent with those genomic analyses, we confirmed the T-bet-dependent regulation of NK1.1 and heterodimers of CD94 and NKG2 in NCR⁺ ILC3 cells at the protein level (**Fig. 1c**). Thus, in addition to being required for the development of NCR⁺ ILC3 cells from NCR⁻ ILC3 cells, T-bet seemed to have a role in the recognition, effector function and migration of NCR⁺ ILC3 cells within tissues. T-bet was also the major driver of the 'NK cell–ness' program of NCR⁺ ILC3 cells.

NCR⁺ ILC3 cells are dispensable in immunocompetent mice

The pathway analysis of ILC3 transcriptomic data revealed that the set of genes expressed in NCR⁺ ILC3 cells and downregulated in *Tbx21*$^{+/-}$ mice showed enrichment for in genes encoding products involved in the control of gastrointestinal disease and bacterial infection (**Fig. 1b**). Consistent with those data, NCR⁺ ILC3 cells are reported to be pivotal in protection against *C. rodentium* in various models of immunodeficient mice[11,13,14,17]. We therefore investigated the role of the IL-22 produced by NCR⁺ ILC3 cells during the course of infection with *C. rodentium* by specifically deleting IL-22 from NCR⁺ cells; thus, NCR⁺ ILC3 cells were targeted, while NCR⁻ ILC3 cells would remain intact. We used a previously undescribed model of mice with sequence encoding enhanced GFP knocked into both alleles (*Il22*$^{eGFP/eGFP}$) and expressing 'improved' Cre recombinase (iCre)

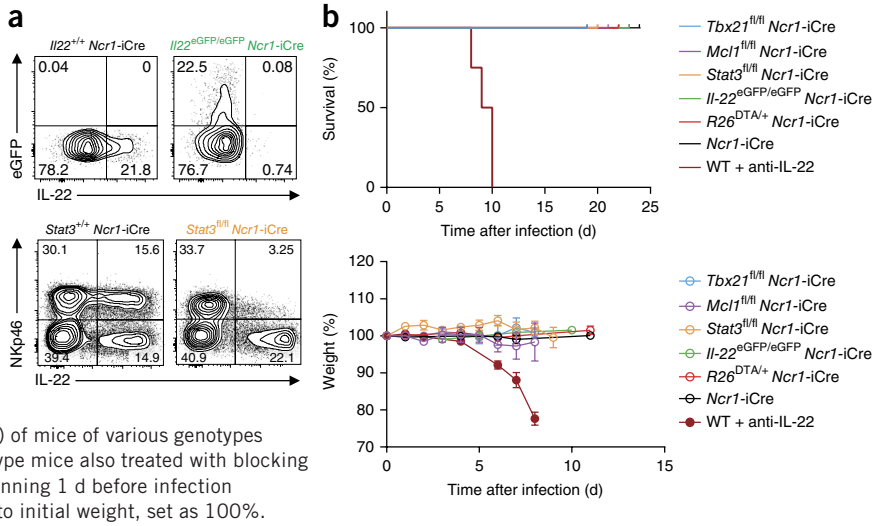

Figure 2 Targeting of NCR⁺ ILC3 cells during infection with *C. rodentium*. (**a**) Flow cytometry analyzing IL-22 in Lin⁻CD45⁺NCR⁺ ILC3 cells obtained from the small intestine of naive *Il22*$^{+/+}$*Ncr1*-iCre mice and *Il22*$^{eGFP/eGFP}$ *Ncr1*-iCre mice and stimulated for 4–5 h *in vitro* with IL-23 in the presence of brefeldin A (top) or in NKp46⁺ or NKp46⁻ lymphocytes obtained from the small intestine of *Stat3*$^{+/+}$*Ncr1*$^{+/+}$*Rorc*$^{+/GFP}$ mice (*Stat3*$^{+/+}$*Ncr1*-iCre) and *Stat3*$^{fl/fl}$*Ncr1*-iCre*Rorc*$^{+/GFP}$ mice (*Stat3*$^{fl/fl}$*Ncr1*-iCre) 8 d after infection with *C. rodentium* and stimulated as above, gated on Lin⁻CD45.2⁺ cells (bottom). Numbers in quadrants indicate percent cells in each. (**b**) Survival (top) and change in body weight (bottom) of mice of various genotypes (key) after infection with *C. rodentium*, and in wild-type mice also treated with blocking monoclonal antibody to anti-IL-22 twice weekly, beginning 1 d before infection (WT + anti-IL-22); body weight is presented relative to initial weight, set as 100%. Data are from one experiment representative of two independent experiments (**a**; $n = 3–4$ mice per genotype in each) or are pooled from five independent experiments (**b**; mean ± s.e.m. of $n = 3–4$ mice per genotype in each).

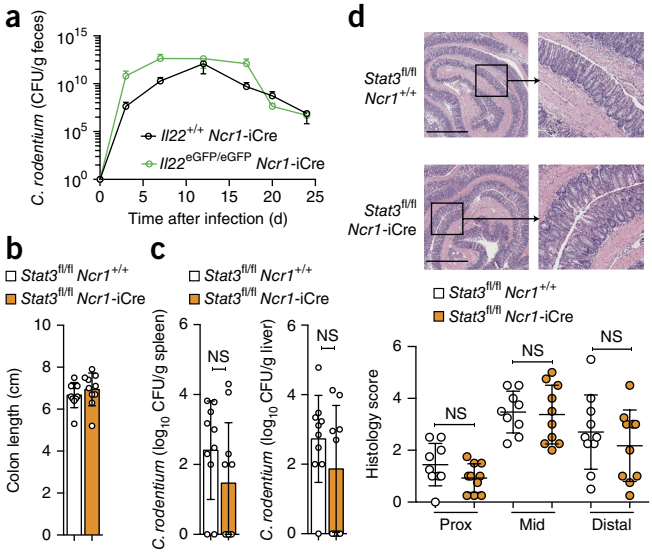

Figure 3 *C. rodentium* infection in the absence of IL-22 production by NCR⁺ ILC3 cells. (**a**) *C. rodentium* in the feces of *Il22*$^{+/+}$*Ncr1*-iCre and *Il22*$^{eGFP/eGFP}$*Ncr1*-iCre mice orally inoculated with 1×10^{10} CFU *C. rodentium* on day 0. (**b**,**c**) Colon length (**b**) and bacterial load in spleen (left) and liver (right) (**c**) of male *Stat3*$^{fl/fl}$*Ncr1*$^{+/+}$ and *Stat3*$^{fl/fl}$*Ncr1*-iCre mice 8 d after oral inoculation with 2×10^9 CFU of *C. rodentium*. (**d**) Pathological features in the colon of the mice as in **b**,**c**, assessed by hematoxylin-and-eosin staining of formalin-fixed paraffin-embedded sections (micrographs) of colons (top), and histological scores of the proximal (Prox), middle (Mid) and distal colon of those mice (below; **Supplementary Table 3**). Areas outlined at left (top) are enlarged 3.4× at right. Scale bars, 1,000 μm (main images). Each symbol (**b**–**d**) represents an individual mouse; small horizontal lines (**c**) indicate the mean (± s.d.). NS, not significant ($P > 0.05$ (unpaired Student's *t*-test)). Data are pooled from three independent experiments (**a**; mean ± s.d. of $n = 4$–6 mice per group in each) or are pooled from three independent experiments (**b**–**d**; mean ± s.d. of $n = 3$–4 mice per group in each).

from the locus encoding NKp46 (*Ncr1*$^{iCre/+}$; called '*Ncr1*-iCre' here) (**Supplementary Fig. 1**); in these mice, NCR⁺ ILC3 cells were unable to produce IL-22 (**Fig. 2a**). We also crossed *Ncr1*-iCre mice with mice with *lox*P-flanked alleles encoding the transcription factor STAT3 (*Stat3*$^{fl/fl}$), for the selective abolition of STAT3-dependent signaling in NCR⁺ ILC3 cells, as STAT3 is required for the production of IL-22 by ILC3 cells and T_H17 cells, and ablation of *Stat3* in RORγt⁺ lymphocytes leads to increased morbidity and mortality after infection with *C. rodentium*[22]. NCR⁺ ILC3 cells from *Il22*$^{eGFP/eGFP}$*Ncr1*-iCre and *Stat3*$^{fl/fl}$*Ncr1*-iCre mice were unable to produce IL-22 (**Fig. 2a**), but both types of mice were resistant to infection with *C. rodentium*, as we observed no death, weight loss, histological abnormalities in the gut or increase in bacterial dissemination in these mice relative to that of *Ncr1*-iCre mice (**Figs. 2b** and **3**). This resistance could not be accounted for by a compensatory increase in IL-22 production by NCR⁻ ILC3 cells, which were present in normal numbers and produced normal amounts of the cytokine (**Supplementary Figs. 1c**,**d** and **2**). In contrast, treatment with blocking antibody to IL-22 led to severe colitis and premature death of wild-type mice challenged with the same dose of *C. rodentium* (**Fig. 2b**), as reported before[16]. Thus, IL-22 was essential for resistance to *C. rodentium*, but the production of IL-22 by NCR⁺ ILC3 cells was dispensable for this.

We then ablated NCR⁺ ILC3 cells to address their contribution to the control of infection with *C. rodentium* more generally. We directly abolished *Tbx21* expression in NCR⁺ ILC3 cells by crossing *Ncr1*-iCre mice with *Tbx21*$^{fl/fl}$ mice to generate *Tbx21*$^{fl/fl}$*Ncr1*-iCre mice. Consistent with findings reported above, the number of NKp46⁺ RORγt⁻ cells and NCR⁺ ILC3 cells was much smaller in the small intestine and colon of *Tbx21*$^{fl/fl}$*Ncr1*-iCre mice than in that of *Tbx21*$^{fl/fl}$*Ncr1*$^{+/+}$ mice (**Fig. 4** and **Supplementary Fig. 3a**). However, *Tbx21*$^{fl/fl}$*Ncr1*-iCre mice were resistant to infection with *C. rodentium*, as we observed no death, weight loss, histological abnormalities in the gut or increase in bacterial dissemination in *Tbx21*$^{fl/fl}$*Ncr1*-iCre mice relative to that of *Tbx21*$^{fl/fl}$*Ncr1*$^{+/+}$ mice (**Fig. 2b** and **Supplementary Fig. 3b**–**d**). We observed a much greater number of IL-22-producing NCR⁻ ILC3 cells in *Tbx21*$^{fl/fl}$*Ncr1*-iCre mice than in *Tbx21*$^{fl/fl}$*Ncr1*$^{+/+}$ mice (**Fig. 4** and **Supplementary Fig. 3a**), which potentially compensated for the loss of NCR⁺ ILC3 cells in this model. We thus addressed the role of ILC3 cells during infection with *C. rodentium* further by generating another model of deficiency in NCR⁺ ILC3 cells by crossing *Ncr1*-iCre mice with mice heterozygous for expression of the gene encoding diphtheria toxin fragment A (DTA) from the ubiquitous Rosa26 locus (*R26*$^{DTA/+}$; *Rosa*-DTA) to generate *R26*$^{DTA/+}$*Ncr1*-iCre mice. We observed a nearly complete absence of NKp46⁺ cells (both NCR⁺ RORγt⁻ cells and NCR⁺ ILC3 cells) in the small

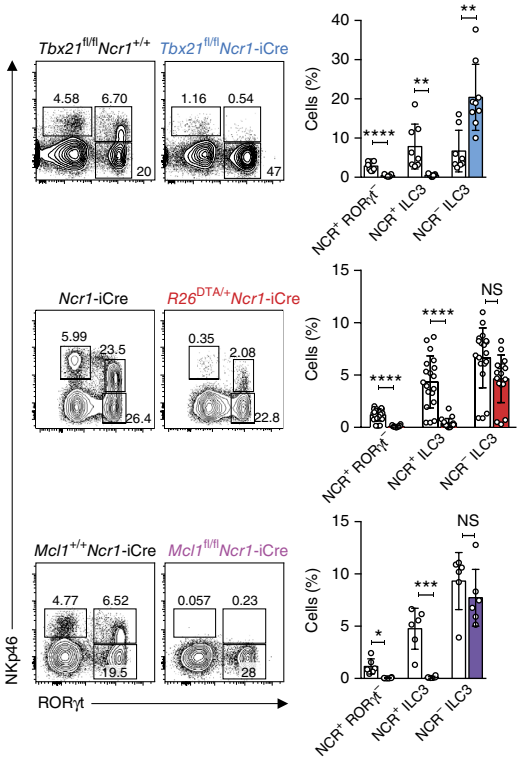

Figure 4 Effect of deletion of *Tbx21* and *Mcl1* or expression of DTA on NCR⁺ ILC3 cells. Flow cytometry analyzing the surface expression of NKp46 and intracellular expression of RORγt by Lin⁻CD45⁺ lymphocytes from the small intestine of naive *Tbx21*$^{fl/fl}$*Ncr1*$^{+/+}$, *Tbx21*$^{fl/fl}$*Ncr1*-iCre, *Ncr1*-iCre, *R26*$^{DTA/+}$*Ncr1*-iCre, *Mcl1*$^{+/+}$*Ncr1*-iCre and *Mcl1*$^{fl/fl}$*Ncr1*-iCre mice. Numbers adjacent to outlined areas (left) indicate percent NKp46⁺ (NCR⁺) RORγt⁻ cells (top left), NKp46⁺ (NCR⁺) RORγt⁺ cells (top right) or NKp46⁻ (NCR⁻) RORγt⁺ cells (bottom right). Right, frequency of NCR⁺RORγt⁻ cells, NCR⁺ ILC3 cells or NCR⁻ ILC3 cells among live cells (colors of bars at far right match colors for genotypes above right plots). Each symbol represents an individual mouse. $^*P < 0.05$, $^{**}P < 0.01$, $^{***}P < 0.001$ and $^{****}P < 0.0001$ (unpaired Student's *t*-test). Data are pooled from at least three independent experiments (mean ± s.d. of $n = 2$–4 mice per group in each).

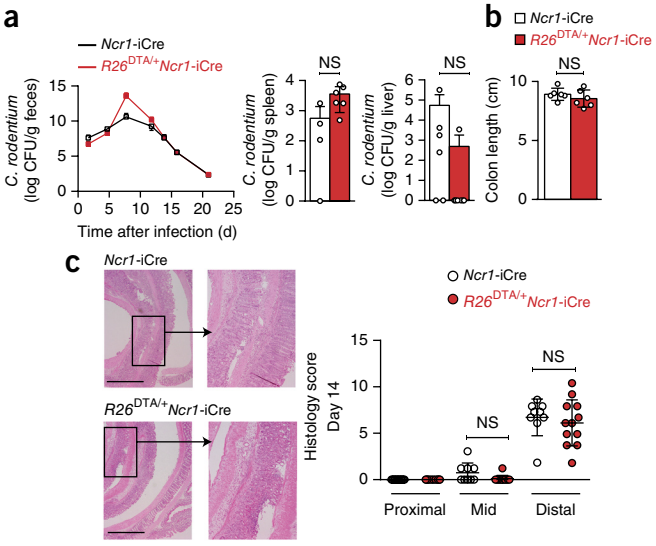

Figure 5 Infection with *C. rodentium* in the absence of NCR$^+$ ILC3 cells. (**a**) Bacterial load of *R26*$^{DTA/+}$*Ncr1*-iCre and *Ncr1*-iCre littermates orally inoculated with 1 × 10^{10} CFU *C. rodentium* on day 0, assessed in the feces over the course of the experiment (left), or in the spleen (middle) and liver (right) at 14 d after infection. (**b**,**c**) Colon length (**b**) and pathological features (**c**; as in **Fig. 3d**) of *R26*$^{DTA/+}$*Ncr1*-iCre and *Ncr1*-iCre mice 14 d after infection as in **a**. Scale bars (**c**), 1,000 µm. Each symbol represents an individual mouse; small horizontal lines (**c**) indicate the mean (± s.d.). *P* values (NS), unpaired Student's *t*-test. Data are representative of three independent experiments (**a**; *n* = 4–8 mice per group) or are pooled from two to three independent experiments (**b**,**c**; *n* = 4–9 mice per genotype, with one to two sections per mouse (**c**, right)).

intestine and colon of *R26*$^{DTA/+}$*Ncr1*-iCre mice, with no greater abundance of NCR$^-$ ILC3 cells in the small intestine and colon of *R26*$^{DTA/+}$*Ncr1*-iCre mice than in that of their *Ncr1*-iCre littermates (**Fig. 4** and **Supplementary Fig. 4a**,**b**). We recorded no morbidity or mortality for *R26*$^{DTA/+}$*Ncr1*-iCre mice infected with *C. rodentium* (**Fig. 2b**). Those findings were supported by a lack of difference between *R26*$^{DTA/+}$*Ncr1*-iCre mice and *Ncr1*-iCre mice in terms of colon length or histology, or bacterial dissemination, as assessed by quantification of colony-forming units (CFU) of *C. rodentium* in the feces, spleen and liver (**Fig. 5**). We further monitored the immune response to *C. rodentium* infection in these mice and we found no differences in other parameters, such as the cellularity of the gut lamina propria for CD4$^+$ T cells, CD8$^+$ T cells, B cells, Ly6G$^+$Ly6C$^+$ myeloid cells and MHCII$^+$CD11c$^+$ dendritic cells, or the ability of mesenteric lymph node and splenic CD4$^+$ T cells and CD8$^+$ T cells to produce IL-17A or interferon-γ (IFN-γ) upon *ex-vivo* stimulation (**Supplementary Fig. 4c–e**). Measurement of cytokines (IFN-γ, IL-17A, Il-1β, IL-6, CXCL1 (KC), TNF and IL-10) in gut extracts revealed no differences between *R26*$^{DTA/+}$*Ncr1*-iCre mice and *Ncr1*-iCre mice (**Supplementary Fig. 4f**).

Mcl-1 is an anti-apoptotic protein induced by signaling via the common γ-chain receptor and is required for the maintenance of NK cells *in vivo*[23]. We investigated whether Mcl-1 was also required for the maintenance of NCR$^+$ ILC3 cells in the gut, through the use of mice with deletion of *lox*P-flanked *Mcl1* alleles by iCre expressed from the *Ncr1* locus (*Mcl1*$^{fl/fl}$*Ncr1*-iCre mice). Both NCR$^+$ RORγt$^-$ cells and NCR$^+$ ILC3 populations were absent from *Mcl1*$^{fl/fl}$*Ncr1*-iCre mice (**Fig. 4**). These data demonstrated a key role for Mcl-1 in the maintenance of all NKp46$^+$ ILCs *in vivo*. *Mcl1*$^{fl/fl}$*Ncr1*-iCre mice represent another model of immunodeficiency in which NCR$^+$ ILC3 cells are absent but NCR$^-$ ILC3 cells and T cells are unaffected. We challenged *Mcl1*$^{fl/fl}$*Ncr1*-iCre mice with *C. rodentium*. As noted for *R26*$^{DTA/+}$*Ncr1*-iCre mice, *Mcl1*$^{fl/fl}$*Ncr1*-iCre mice were resistant to the infection (**Fig. 2b**), with no sign of disease or bacterial dissemination detected by histology or on the basis of colon length or CFU in the spleen and liver (**Supplementary Fig. 5**). Thus, results obtained with five different genetic models converged to reveal that NCR$^+$ ILC3 cells were dispensable for the control of *C. rodentium* infection in immunocompetent mice.

The diminished production of IL-22 by ILC3 cells in mice deficient in the transcription factor AhR allows the proliferation of commensal segmented filamentous bacteria, which are known to promote the development of T_H17 cells[24]. We therefore also investigated the consequences of a lack of NCR$^+$ ILC3 cells for gut microbiota at steady state, by deep sequencing. We detected no difference in the presence of particular bacterial families or number of segmented filamentous bacteria in the feces, or in the number of T_H17 cells in the small intestine, in comparisons of *R26*$^{DTA/+}$*Ncr1*-iCre mice and *Ncr1*-iCre mice housed in the same conditions (**Supplementary Fig. 6a–c**). Similarly, the bacterial families present in the gut of *Mcl1*$^{fl/fl}$*Ncr1*-iCre mice did not differ from those present in the gut of *Ncr1*-iCre mice (data not shown). Thus, a deficiency in NCR$^+$ ILC3 cells had no effect on the gut microbiota in immunocompetent hosts at steady state.

A role for NCR$^+$ ILC3 cells in immunodeficient mice

The results presented above contrasted with published reports of a critical role for NCR$^+$ ILC3 cells in protection against *C. rodentium* in mice deficient in the gene encoding the RAG recombinase component RAG-2 (*Rag2*), T-bet (*Tbx21*), the chemokine receptor CXCR6 (*Cxcr6*) or the transcription factor Id2 (*Id2*)[11,13,14,17,25]. As all these mouse models display profound or partial immunodeficiency, we investigated the role of NCR$^+$ ILC3 cells in immunodeficient and immunocompetent mice directly, by crossing *R26*$^{DTA/+}$*Ncr1*-iCre mice with *Rag2*$^{-/-}$ mice, which lack T cells and B cells. We then infected *Rag2*$^{-/-}$ *Ncr1*-iCre mice and *Rag2*$^{-/-}$*R26*$^{DTA/+}$*Ncr1*-iCre and *R26*$^{DTA/+}$*Ncr1*-iCre littermates with *C. rodentium* and evaluated their resistance to bacterial infection by monitoring mouse weight and survival. Consistent with our findings reported above, *R26*$^{DTA/+}$*Ncr1*-iCre mice were resistant to *C. rodentium* (**Fig. 6**). After initial

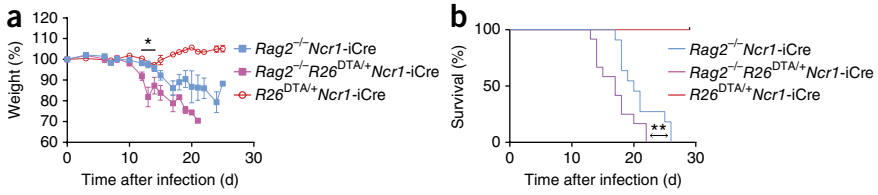

Figure 6 Role of NCR$^+$ ILC3 cells in immunocompetent and immunodeficient hosts during infection with *C. rodentium*. Change in body weight (**a**) and survival (**b**) of *Rag2*$^{-/-}$*Ncr1*-iCre mice and of *Rag2*$^{-/-}$*R26*$^{DTA/+}$*Ncr1*-iCre and *R26*$^{DTA/+}$*Ncr1*-iCre littermates following infection with *C. rodentium*. *$P < 0.04$, *Rag2*$^{-/-}$*R26*$^{DTA/+}$*Ncr1*-iCre versus *R26*$^{DTA/+}$*Ncr1*-iCre at days 12, 13 and 14 after infection (**a**) and **$P < 0.001$ (unpaired Student's *t*-test (**a**) or log-rank Mantel-Cox test (**b**)). Data are pooled from two independent experiments (*n* = 3–11 mice per genotype; mean ± s.e.m. in **a**).

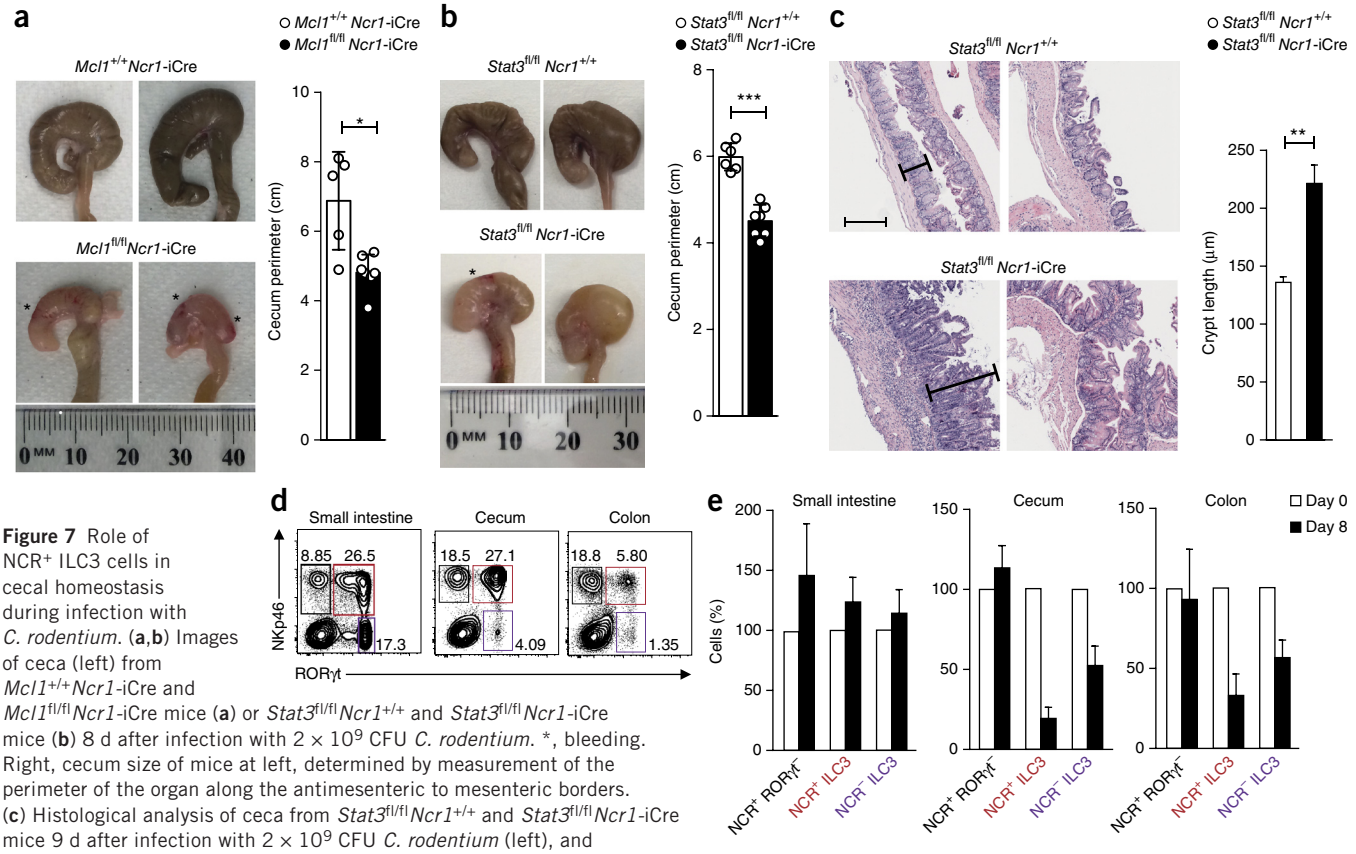

Figure 7 Role of NCR⁺ ILC3 cells in cecal homeostasis during infection with *C. rodentium*. (**a**,**b**) Images of ceca (left) from *Mcl1*$^{+/+}$*Ncr1*-iCre and *Mcl1*$^{fl/fl}$*Ncr1*-iCre mice (**a**) or *Stat3*$^{fl/fl}$*Ncr1*$^{+/+}$ and *Stat3*$^{fl/fl}$*Ncr1*-iCre mice (**b**) 8 d after infection with 2×10^9 CFU *C. rodentium*. *, bleeding. Right, cecum size of mice at left, determined by measurement of the perimeter of the organ along the antimesenteric to mesenteric borders. (**c**) Histological analysis of ceca from *Stat3*$^{fl/fl}$*Ncr1*$^{+/+}$ and *Stat3*$^{fl/fl}$*Ncr1*-iCre mice 9 d after infection with 2×10^9 CFU *C. rodentium* (left), and quantification of cecal crypt length in those mice (right). Bracketed lines spanning crypts (left) indicate relative length of crypts. Scale bar (bottom left corner, top left), 500 μM. (**d**) Flow cytometry analyzing the expression of RORγt-GFP and surface expression of NKp46 by Lin⁻CD45⁺ cells isolated from the lamina propria of the small intestine, cecum and colon of naive *Rorc*$^{+/GFP}$ mice. Numbers adjacent to outlined areas indicate percent NKp46⁺ (NCR⁺) RORγt⁻ cells (top left), NKp46⁺ (NCR⁺) RORγt⁺ cells (top right) or NKp46⁻ (NCR⁻) RORγt⁺ cells (top left). (**e**) Frequency of NCR⁺RORγt⁻ cells, NCR⁺ ILC3 cells or NCR⁻ ILC3 cells in wild-type mice on day 0 (set as 100%) and day 8 after infection with 1×10^{10} CFU *C. rodentium*. Each symbol (**a**,**b**) represents an individual mouse. $*P < 0.01$, $**P < 0.001$ and $***P < 0.0001$ (unpaired Student's *t*-test). Data are pooled from two independent experiments (**a**–**c**; mean ± s.d. of $n = 2$–4 (**a**) or 3–4 (**b**) mice per genotype in each or $n = 8$ mice per genotype (**c**)), are representative of two independent experiments (**d**; $n = 3$ mice per group in each) or are from one experiment representative of two independent experiments (**e**; mean and s.d. of $n = 6$ mice).

control of the infection, *Rag2*$^{-/-}$*Ncr1*-iCre mice lost weight and started to succumb to the disease on day 17 after infection (**Fig. 6**), as reported before[26]. *Rag2*$^{-/-}$*R26*$^{DTA/+}$*Ncr1*-iCre mice were even more susceptible to the infection than were their *Rag2*$^{-/-}$*Ncr1*-iCre littermates, as shown by their greater weight loss on days 12–14 after infection, with the first mice dying on day 13 and all mice dead by day 22, in contrast to the death of all *Rag2*$^{-/-}$*Ncr1*-iCre mice by day 26 (**Fig. 6**). Thus, NCR⁺ ILC3 cells were not essential for the control of *C. rodentium* in immunocompetent hosts, whereas they contributed to the control of *C. rodentium* in immunodeficient mice.

A role for NCR⁺ ILC3 cells in cecal homeostasis

In contrast to the lack of effect of deficiency in NCR⁺ ILC3 cells in the small intestine or the bulk of the colon, the absence of NCR⁺ ILC3 cells in *Mcl1*$^{fl/fl}$*Ncr1*-iCre mice during infection with *C. rodentium* resulted in a smaller cecum than that of wild-type mice, together with ulceration and bleeding (**Fig. 7a**). We also observed those pathological features in the cecum of *Stat3*$^{fl/fl}$*Ncr1*-iCre mice infected with *C. rodentium* (**Fig. 7b**). Those features were accompanied by crypt hyperplasia and inflammation, as shown by the staining of cecal sections with hematoxylin and eosin (**Fig. 7c**). We observed no alteration in the cecum, small intestine or colon at steady state in any of the five genetic models of deficiency in NCR⁺ ILC3 cells (*Mcl1*$^{fl/fl}$*Ncr1*-iCre, *R26*$^{DTA/+}$*Ncr1*-iCre, *Tbx21*$^{fl/fl}$*Ncr1*-iCre, *Il22*$^{eGFP/eGFP}$*Ncr1*-iCre or *Stat3*$^{fl/fl}$*Ncr1*-iCre) (data not shown). Thus, NCR⁺ ILC3 cells had a role in protecting the cecum during *C. rodentium* infection, and this function was abolished in conditions in which NCR⁺ ILC3 cells were unable to produce IL-22.

We further delineated the role of NKp46⁺ cells in the control of cecal homeostasis during infection with *C. rodentium* by assessing the regional distribution of gut ILCs. *C. rodentium* is a colonic infection, but it begins in the cecum. In wild-type mice, the protective role of NKp46⁺ cells was associated with a high frequency of NCR⁺ ILC3 cells in the cecum at steady state, in contrast to the low frequency of NCR⁺ ILC3 cells in the colon (**Fig. 7d**). At the junction of the small intestine and the colon, the cecum was globally characterized by a distribution of ILCs with features of both the small intestine, with a high frequency of NCR⁺ ILC3 cells, and the colon, with a low frequency of NCR⁻ ILC3 cells (**Fig. 7d**). In wild-type mice, this distribution of intestinal ILCs underwent profound alteration over the course of *C. rodentium* infection, as the frequency of NCR⁺ ILC3 cells was considerably lower in the cecum and colon (**Fig. 7e**). The causes and consequences of these changes remain to be fully explored. A characteristic feature of cecal NCR⁺ ILC3 cells is their high density of cell-surface expression of NK1.1, in contrast to the low density of NK1.1 at the surface of NCR⁺ ILC3 cells in the small intestine and its intermediate expression on NCR⁺ ILC3 cells in the colon (**Supplementary Fig. 7a**). The role of NK1.1 is unknown,

but these data provide an explanation for the reported deleterious effect of treatment with antibody to NK1.1 on *Rag2*$^{-/-}$ mice infected with *C. rodentium*[14]. Indeed, treatment with depleting antibody to NK1.1 decreased the number of NCR$^+$ ILC3 cells, particularly in the cecum, but also in the colon to some extent, whereas it had no effect on the number of NCR$^+$ ILC3 cells in the small intestine (**Supplementary Fig. 7b**). Treatment with antibody to NK1.1 also resulted in depletion of NKp46$^+$RORγt$^-$ cells, including NK cells, ILC1 cells and 'ex-ILC3' (formerly ILC3) cells (**Supplementary Fig. 7b**). However, all NKp46$^+$RORγt$^-$ cells produce IFN-γ, and IFN-γ-deficient mice are not more sensitive to *C. rodentium* infection[26], in contrast to IL-22-deficient mice[16]. Overall, these results suggested that cecal NK1.1$^+$ NCR$^+$ ILC3 cells were involved in the control of infection with *C. rodentium*, through their production of IL-22.

DISCUSSION

The aim of this study was to delineate the biology of NCR$^+$ ILC3 cells, a subset of IL-22-producing ILCs of the gut, and their interplay with adaptive immunity in the context of a colonic infection, in the *C. rodentium* model. By using *Ncr1*-iCre mice, in which NCR$^+$ cells are selectively targeted, we were able to highlight the intrinsic roles of the molecules encoded by *Tbx21*, *Mcl1* and *Stat3* in the development, maintenance and function of NCR$^+$ ILC3 cells. The generation of *Il22*$^{eGFP/eGFP}$*Ncr1*-iCre mice also made it possible to carry out functional fate mapping of IL-22-producing NCR$^+$ ILC3 cells, without detectable cofounding effects due to under-reporting of the *Il22*-Cre transgene[27]. Using these mice, we detected no IL-22 production by intestinal RORγt$^-$NKp46$^+$ cells, including NK cells, ILC1 cells and 'ex-ILC3' cells[28]. Our findings contrast with those of other studies reporting the production of IL-22 by human and mouse NK cells from various inflamed tissues[29–33] and lead us to reconsider whether RORγt$^-$ ILCs might produce IL-22.

We also showed that neither the production of IL-22 by NCR$^+$ ILC3 cells nor the cells themselves were essential for the control of intestinal infection by *C. rodentium* in immunocompetent hosts. In these mice, NCR$^+$ ILC3 cells did not control the gut commensal microbiota either. Published studies have shown that NCR$^+$ ILC3 cells have a critical role in protection against *C. rodentium* in mice with profound or partial immunodeficiency[11,13,14,17]. Our results are consistent with published reports[10,34] and challenge the current dogma in revealing that NCR$^+$ ILC3 cells were not essential for the control of intestinal infection in the presence of T cells. We also found that NCR$^+$ ILC3 cells were able to confer some protection against *C. rodentium* when T cells were absent. The critical role of IL-22-producing T cells in the control of *C. rodentium* infection has already been demonstrated[26]. Published studies have investigated the contributions of T_H17 cells and T_H22 cells during the late phases of *C. rodentium* infection[26] and have suggested that the IL-22 produced by the total ILC3 population (consisting of multiple subsets) is important early in *C. rodentium* infection, but that once T cells are activated, ILC3 cells seem to be dispensable[13,16,22,26,27,35]. Thus, NCR$^+$ ILC3 cells, NCR$^-$ ILC3 cells and T_H17 or T_H22 cells can display some functional redundancy. It has also been suggested that NCR$^-$ ILC3 cells provide an adequate barrier to *C. rodentium* infection[36], as they produce large amounts of IL-22 in the gut[27]. However, we found here that these cells were not sufficient to confer protection against *C. rodentium* in T cell–compromised mice in the presence or absence of NCR$^+$ ILC3 cells. Nevertheless, formal elucidation of the role of NCR$^-$ ILC3 cells in the control of the gut commensal and pathogenic microbiota awaits the development of tools for the selective ablation of this cell population.

The interplay between T cells and ILCs is a matter of great interest. ILCs can interact with CD4$^+$ T cells via major histocompatibility complex class II molecules, which limits the pathological responses of cells of the adaptive immune system to commensal bacteria[37]. It has also been suggested that T cells function as antigen-specific sensors for the activation of ILCs, to amplify and 'instruct' local immune responses[38]. We have described here another type of relationship between T cells and ILC3 cells in which NCR$^+$ ILC3 cells partly overcame the lack of T cells for protection against the pathogenic bacterium *C. rodentium* but became redundant when T cells were present. This is, to our knowledge, the first formal demonstration of redundancy between T cells and ILCs. T cells and ILCs have evolved similar effector functions despite their use of different recognition strategies: a germline-encoded receptor for ILCs, and antigen receptors generated by site-specific somatic recombination for T cells. We thus speculate that ILC3 cells and T_H17 or T_H22 cells have evolved together, which has led to the selection of robust failsafe mechanisms for ensuring adequate control of commensal gut microbiota and protection against intestinal infections. Selective pressure for redundancy might have led to the similarities between ILCs and T cells in terms of their distribution and effector function.

Unexpectedly, we observed severe pathological features in the cecum after the ablation of NCR$^+$ ILC3 cells. Similar severe cecal lesions have also been observed in IL-22-deficient mice after infection with *C. rodentium*[16], in support of the possibility of a role for NCR$^+$ ILC3 cells, the only NKp46$^+$ cells that can produce IL-22, in the altered cecal phenotype. The cecum is the first site in the gastrointestinal tract to be colonized by *C. rodentium* during infection, with invasion of the colon occurring later (at approximately day 8) (ref. 39). We thus propose a model in which NCR$^+$ ILC3 cells are redundant with T cells for protection against lethality and colon disease during intestinal infection but are critical for protection against cecal damage at the earliest stage of infection. The cecum is a blind pouch at the junction between the small intestine and the large intestine. It is a source of bacteria and is also linked to the appendix in humans and mice, in which it is referred to as the 'cecal patch'. The appendix has generally been seen as a vestige of evolution, but phylogenetic studies have challenged the apparent lack of function of the cecum and appendix[40]. In particular, it has been suggested that the cecum and appendix provide an important reservoir for maintenance of the gut flora, which is anatomically protected from the intestinal lumen and might allow seeding of the gut after dysbiosis. Our data demonstrating a critical role for NCR$^+$ ILC3 cells in the homeostasis of the cecum upon bacterial infection opens up new possibilities for delineating the role of ILC3 cells in the pathophysiology of the cecum and appendix and in maintaining the health of the intestinal tract. In particular, future studies should determine whether the balance between NCR$^-$ ILC3 cells and NCR$^+$ ILC3 cells is involved in the still-unknown mechanisms that lead to appendicitis and resistance or susceptibility to inflammatory bowel diseases, as these two conditions might be related[41].

METHODS

Methods and any associated references are available in the online version of the paper.

Accession codes. GEO: RNA-seq, GSE72909; NCBI BioProject, PRJNA295954.

Note: Any Supplementary Information and Source Data files are available in the online version of the paper.

ACKNOWLEDGMENTS

We thank M. Camilleri, J. Vella, E. Loza and L. Inglis and the staff of the animal and flow cytometry facilities of The Walter and Eliza Hall Institute of Medical Research and the Centre d'Immunologie de Marseille-Luminy for technical assistance; S. Kaech (Yale University) for mice with *lox*P-flanked alleles encoding T-bet; and L. Chasson and C. Laprie (Centre d'Immunologie de Marseille-Luminy) for expertise in histology and for assigning scores to tissue sections. Supported by the National Health and Medical Research Council of Australia (G.T.B., Se.C. and N.H.; Dora Lush Postgraduate Research Scholarship to L.C.R.); the Australian Research Council (Future Fellowship to G.T.B.); the Victorian State Government Operational Infrastructure Support and Australian Government National Health and Medical Research Council Independent Research Institutes Infrustructure Support; the European Research Council (THINK Advanced Grant), the Ligue Nationale contre le Cancer (Equipe Labellisée), INSERM, CNRS and Aix-Marseille University to Centre d'Immunologie de Marseille-Luminy (all for the E.V. laboratory); and the Institut Universitaire de France (E.V.).

AUTHOR CONTRIBUTIONS

C.S., L.A.M. and Y.K. contributed equally to this work; L.C.R., M.J.H.G.-M., C.S., L.A.M. and Y.K. designed the research, performed experiments and analyzed the data; A.F., E.W., S.M., L.M., J.G., T.P. and A.T.P. performed experiments and analyzed the data; W.S. and G.K.S. performed bioinformatics analyses of RNA-seq data; O.L., D.D., M.L., J.-C.R., C.A., S.U., Se.C. and N.D.H. provided reagents; and G.T.B. and E.V. designed the research, supervised the study, and wrote the manuscript with the help of the other co-authors.

COMPETING FINANCIAL INTERESTS

The authors declare competing financial interests: details are available in the online version of the paper.

1. Dudakov, J.A., Hanash, A.M. & van den Brink, M.R. Interleukin-22: immunobiology and pathology. *Annu. Rev. Immunol.* **33**, 747–785 (2015).
2. Spits, H. *et al.* Innate lymphoid cells–a proposal for uniform nomenclature. *Nat. Rev. Immunol.* **13**, 145–149 (2013).
3. McKenzie, A.N., Spits, H. & Eberl, G. Innate lymphoid cells in inflammation and immunity. *Immunity* **41**, 366–374 (2014).
4. Diefenbach, A., Colonna, M. & Koyasu, S. Development, differentiation, and diversity of innate lymphoid cells. *Immunity* **41**, 354–365 (2014).
5. Montaldo, E., Juelke, K. & Romagnani, C. Group 3 innate lymphoid cells (ILC3s): Origin, differentiation, and plasticity in humans and mice. *Eur. J. Immunol.* **45**, 2171–2182 (2015).
6. Eberl, G., Di Santo, J.P. & Vivier, E. The brave new world of innate lymphoid cells. *Nat. Immunol.* **16**, 1–5 (2015).
7. Eberl, G., Colonna, M., Di Santo, J.P. & McKenzie, A.N. Innate lymphoid cells: a new paradigm in immunology. *Science* **348**, aaa6566 (2015).
8. Mebius, R.E., Rennert, P. & Weissman, I.L. Developing lymph nodes collect $CD4^+CD3^-$ $LT\beta^+$ cells that can differentiate to APC, NK cells, and follicular cells but not T or B cells. *Immunity* **7**, 493–504 (1997).
9. Constantinides, M.G. *et al.* PLZF expression maps the early stages of ILC1 lineage development. *Proc. Natl. Acad. Sci. USA* **112**, 5123–5128 (2015).
10. Klose, C.S. *et al.* A T-bet gradient controls the fate and function of CCR6-$ROR\gamma t^+$ innate lymphoid cells. *Nature* **494**, 261–265 (2013).
11. Rankin, L.C. *et al.* The transcription factor T-bet is essential for the development of $NKp46^+$ innate lymphocytes via the Notch pathway. *Nat. Immunol.* **14**, 389–395 (2013).
12. Kirchberger, S. *et al.* Innate lymphoid cells sustain colon cancer through production of interleukin-22 in a mouse model. *J. Exp. Med.* **210**, 917–931 (2013).
13. Satoh-Takayama, N. *et al.* Microbial flora drives interleukin 22 production in intestinal $NKp46^+$ cells that provide innate mucosal immune defense. *Immunity* **29**, 958–970 (2008).
14. Cella, M. *et al.* A human natural killer cell subset provides an innate source of IL-22 for mucosal immunity. *Nature* **457**, 722–725 (2009).
15. Sonnenberg, G.F., Fouser, L.A. & Artis, D. Functional biology of the IL-22-IL-22R pathway in regulating immunity and inflammation at barrier surfaces. *Adv. Immunol.* **107**, 1–29 (2010).
16. Zheng, Y. *et al.* Interleukin-22 mediates early host defense against attaching and effacing bacterial pathogens. *Nat. Med.* **14**, 282–289 (2008).
17. Satoh-Takayama, N. *et al.* The chemokine receptor CXCR6 controls the functional topography of interleukin-22 producing intestinal innate lymphoid cells. *Immunity* **41**, 776–788 (2014).
18. Artis, D. & Spits, H. The biology of innate lymphoid cells. *Nature* **517**, 293–301 (2015).
19. van de Pavert, S.A. & Vivier, E. Differentiation and function of group 3 innate lymphoid cells, from embryo to adult. *Int. Immunol.* doi:10.1093/intimm/dxv052 (22 September 2015).
20. Robinette, M.L. *et al.* Transcriptional programs define molecular characteristics of innate lymphoid cell classes and subsets. *Nat. Immunol.* **16**, 306–317 (2015).
21. Sciumé, G. *et al.* Distinct requirements for T-bet in gut innate lymphoid cells. *J. Exp. Med.* **209**, 2331–2338 (2012).
22. Guo, X. *et al.* Induction of innate lymphoid cell-derived interleukin-22 by the transcription factor STAT3 mediates protection against intestinal infection. *Immunity* **40**, 25–39 (2014).
23. Sathe, P. *et al.* Innate immunodeficiency following genetic ablation of Mcl1 in natural killer cells. *Nat. Commun.* **5**, 4539 (2014).
24. Qiu, J. *et al.* Group 3 innate lymphoid cells inhibit T-cell-mediated intestinal inflammation through aryl hydrocarbon receptor signaling and regulation of microflora. *Immunity* **39**, 386–399 (2013).
25. Guo, X. *et al.* Innate lymphoid cells control early colonization resistance against intestinal pathogens through ID2-dependent regulation of the microbiota. *Immunity* **42**, 731–743 (2015).
26. Basu, R. *et al.* Th22 cells are an important source of IL-22 for host protection against enteropathogenic bacteria. *Immunity* **37**, 1061–1075 (2012).
27. Ahlfors, H. *et al.* IL-22 fate reporter reveals origin and control of IL-22 production in homeostasis and infection. *J. Immunol.* **193**, 4602–4613 (2014).
28. Vonarbourg, C. *et al.* Regulated expression of nuclear receptor $ROR\gamma t$ confers distinct functional fates to NK cell receptor-expressing $ROR\gamma t^+$ innate lymphocytes. *Immunity* **33**, 736–751 (2010).
29. Dhiman, R. *et al.* IL-22 produced by human NK cells inhibits growth of Mycobacterium tuberculosis by enhancing phagolysosomal fusion. *J. Immunol.* **183**, 6639–6645 (2009).
30. Guo, H. & Topham, D.J. Interleukin-22 (IL-22) production by pulmonary Natural killer cells and the potential role of IL-22 during primary influenza virus infection. *J. Virol.* **84**, 7750–7759 (2010).
31. Male, V. *et al.* Immature NK cells, capable of producing IL-22, are present in human uterine mucosa. *J. Immunol.* **185**, 3913–3918 (2010).
32. Tang, Q. *et al.* Development of IL-22-producing NK lineage cells from umbilical cord blood hematopoietic stem cells in the absence of secondary lymphoid tissue. *Blood* **117**, 4052–4055 (2011).
33. Xu, X. *et al.* Conventional NK cells can produce IL-22 and promote host defense in *Klebsiella pneumoniae* pneumonia. *J. Immunol.* **192**, 1778–1786 (2014).
34. Macho-Fernandez, E. *et al.* Lymphotoxin β receptor signaling limits mucosal damage through driving IL-23 production by epithelial cells. *Mucosal Immunol.* **8**, 403–413 (2015).
35. Sonnenberg, G.F. *et al.* Innate lymphoid cells promote anatomical containment of lymphoid-resident commensal bacteria. *Science* **336**, 1321–1325 (2012).
36. Sonnenberg, G.F., Monticelli, L.A., Elloso, M.M., Fouser, L.A. & Artis, D. $CD4^+$ lymphoid tissue-inducer cells promote innate immunity in the gut. *Immunity* **34**, 122–134 (2011).
37. Hepworth, M.R. *et al.* Innate lymphoid cells regulate $CD4^+$ T-cell responses to intestinal commensal bacteria. *Nature* **498**, 113–117 (2013).
38. Gasteiger, G. & Rudensky, A.Y. Interactions between innate and adaptive lymphocytes. *Nat. Rev. Immunol.* **14**, 631–639 (2014).
39. Wiles, S. *et al.* Organ specificity, colonization and clearance dynamics in vivo following oral challenges with the murine pathogen *Citrobacter rodentium*. *Cell. Microbiol.* **6**, 963–972 (2004).
40. Smith, H.F. *et al.* Comparative anatomy and phylogenetic distribution of the mammalian cecal appendix. *J. Evol. Biol.* **22**, 1984–1999 (2009).
41. Frisch, M., Pedersen, B.V. & Andersson, R.E. Appendicitis, mesenteric lymphadenitis, and subsequent risk of ulcerative colitis: cohort studies in Sweden and Denmark. *Br. Med. J.* **338**, b716 (2009).

ONLINE METHODS

Mice. All the mice used were bred and maintained in specific pathogen–free facilities at the Walter and Eliza Hall Institute of Medical Research or Centre d'Immunologie de Marseille-Luminy. C57BL/6 mice, *Rag2*$^{tm1.1Flv}$*Il2rg*$^{tm1.1Flv}$ (Rag2γ_c) mice, *Stat3*$^{fl/fl}$ mice[42], *Rorc*$^{+/GFP}$ mice[43], *Tbx21*$^{-/-}$ [44], *Mcl1*$^{fl/fl}$ mice[23], *Ncr1*-iCre mice[45], *R26*$^{DTA/+}$ (Rosa-DTA) mice and *Rag2*$^{-/-}$*R26*$^{DTA/+}$ mice were used. All animal experiments were performed with the approval of either the Animal Ethics Committees of the Walter and Eliza Hall Institute according to National Health and Medical Research Council of Australia guidelines, or the Animal Ethics Committees of the Centre d'Immunologie de Marseille-Luminy and in accordance with European laws.

Generation of *Il22*$^{fl/fl}$ mice. A *lox*P site was inserted downstream from *Il22* exon 1 and a reporter-selection cassette (loxP-SA-P2A-DTR-T2A-eGFP-polyA-frt-Hyg-frt) was inserted downstream of the *Il22* poly(A) sequence (**Supplementary Fig. 1a**). The genomic coordinates for the *lox*P-flanked region were as follows: 117,642,470–117,647,823, NCBIM37, chromosome 10. *Il22*$^{eGFP/eGFP}$*Ncr1*-iCre mice were obtained at the expected Mendelian frequencies and developed normally and were fertile.

Inoculation with *C. rodentium*. Overnight cultures of bacterial strains were centrifuged and the pellet was resuspended in PBS. Food was withdrawn for 8 h before infection, and the 6- to 9-week-old mice (male and female) were inoculated by oral gavage with 200 µl of a suspension of 2×10^9 or 1×10^{10} CFU of *C. rodentium*. The viable count of the inoculum was determined retrospectively by plating of dilutions of the inoculum on plates with appropriate antibiotics, or on McConkey agar plates (CM0007B; Oxoid) supplemented with 0.68% sodium thiosulfate (Sigma) and 0.08% ammonium citrate (Sigma). Animals were allocated to experimental groups to ensure even distribution of age, sex and weight. Infection experiments were carried out at least twice regardless of sample size, to ensure reproducibility, and results correspond to combined experimental data from all repeats. Mice were weighed daily and feces were collected at 2- to 4-day intervals for bacterial counts. The viable bacterial count per 100 mg of feces was determined by plating of serial dilutions feces, in duplicate, on medium containing selective antibiotics. The colon and small intestine were then collected and their lengths were measured. For assessment of bacterial dissemination, the spleen and liver were collected from infected mice, then were weighed and homogenized. The homogenates were then cultured overnight at 37 °C on LB agar plates containing 10 mM naladixic acid or McConkey agar plates, as described above.

Isolation of lymphoid cells. Intestinal lymphoid cells were isolated from the intestine by incubation one or two times for 20–30 min at 37 °C in Ca^{2+}- and Mg^{2+}-free Hanks medium plus 1 mM EDTA or in PBS supplemented with 1 mM EDTA, 15 mM HEPES and 10% FCS, with gentle shaking for removal of intestinal epithelial cells. Supernatants were discarded and tissues were then incubated, with gentle shaking, twice for 30 min or once for 45 min in 1–1.5 mg/ml (wt/vol) collagenase type III (Worthington), 200 µg/ml DNase I (Roche), 0.4 units/ml Dispase (Gibco) in mouse tonicity RPMI-1640 medium plus 2% (vol/vol) FCS, or for 45 min at 37 °C in RPMI meium supplemented with 15 mM HEPES and 300 units/ml collagenase type VIII (Sigma). Preparations were filtered and mononuclear cells were isolated on a 40%-80% or 90%-100% Percoll gradient. Lymphocytes were recovered from the interface and were washed twice. Mesenteric lymph nodes and splenic lymphoid cells were isolated by mashing of organs on 70-µm filters and resuspension of the material retained on the filter in PBS supplemented with 1 mM EDTA.

***In vitro* T cell restimulation.** Mesenteric lymph node or splenic cells were cultured for 4 h in complete RPMI medium in the presence of PMA (phorbol 12-myristate 13-acetate) (200 ng/ml), ionomycin (1 µg/ml) and BD GolgiStop and GolgiPlug (1:1,000 dilution) (BD Biosciences) for analysis of intracellular cytokines.

Flow cytometry. For analysis of surface molecules, cells were stained with the following antibodies: anti-CD19 (1D3), anti-CD3ε (1452C11), anti-NKp46 (29A1.4), anti-CD4 (GK1.4), anti-NK1.1 (PK136), anti-NKG2A/E/C (20d5), anti-CD94 (18d3), anti-KLRG-1 (2F1) and anti-CD11c (N418) (all from eBioscience); anti-CD45.2 (104), anti-CD117 (2B8), anti-CD8α (53-6.7), anti-I-A/I-E (M5/114.15.2), antiLy6C (AL-21) and anti-Ly6G (1A8) (all from BD Biosciences); and anti-CD49b (DX5; generated at the hybridoma facility of The Walter and Eliza Hall Institute of Medical Research). Live cells were identified by exclusion (by staining with propidium iodide) or with a fixable blue dead cell stain kit (Invitrogen). For intracellular staining, cells were stained for surface markers and with Fixable Viability Dye (eBiosciences), then were fixed and permeabilized with either an intracellular staining kit (eBioscience) or a Cytofix/Cytoperm kit (BD Biosciences). Intracellular staining was then carried out with anti-Rorγt (Q31-378 (BD Biosciences) or AFKJS-9 (eBiosciences)) and anti-T-bet (eBio4B10; eBioscience), for transcription factor analysis, or with anti-IL-22 (IL22JOP (eBioscience) or provided by J.C.R.), coupled to Alexa Fluor 647 with an antibody labeling kit (Life Technologies), and anti-IFN-γ (XMG1.2; BD Bioscience) and anti-IL-17A (TC11-18h10; BD Bioscience), for cytokine analysis. IL-22 production was induced by stimulation of cells for 4-5 h at 37 °C with IL-23 (10-40 ng/ml) in the presence of BD GolgiStop and BD GolgiPlug (1:1000) (BD Biosciences) in complete RPMI-1640 medium (containing 10% FCS, 50 mM 2-mercaptoethanol, 1 mM L-glutamine, 100 U/ml penicillin and 100 µg/ml streptomycin). Flow cytometry was performed with a CantoII, LSRFortessa X-20 or LSR-II cytometer (BD Biosciences) and FlowJo analysis software (Freestar).

Cell purification. Lymphocytes from the lamina propria of the small intestine (pooled from three to six mice) were stained with antibodies to surface markers (identified above), and cells were purified with a BD FACSAria cell sorter (BD Biosciences). Cells were sorted into 50% (vol/vol) FCS/PBS or the appropriate cell culture medium in tubes previously coated with heat-inactivated FCS.

RNA-seq analysis. Total RNA for was prepared from purified ILC populations with an RNeasy mini kit (Qiagen). We generated cDNA from total RNA with OligodT primers and Thermoscript reverse transcriptase (Invitrogen). Quantitative PCR was then performed with a SensiMix SYBR no-Rox kit (Bioline). Approximately 5×10^5 Lin$^-$ (CD3$^-$CD19$^-$) CD45.2$^+$ cells from each ILC subset were sorted from the intestines of *Rorc*$^{+/GFP}$ and *Rorc*$^{+/GFP}$*Tbx21*$^{+/-}$ mice; two biological replicates were generated and subjected to 50–base pair single-end sequencing on an Illumina HiSeq2000 at the Australian Genome Research Facility. More than 30×10^6 reads were generated for each replicate and were aligned with the GRCm38 mm10 build of the *Mus musculus* genome, through the use of the Subread aligner[46]. Gene-wise counts were obtained with the featureCounts program[47]. Reads overlapping exons in annotation build 38.1 of the NCBI RefSeq database were included. Genes were filtered out and excluded from downstream analysis if they failed to achieve a CPM value (counts per million mapped reads) of at least 0.5 in at least two libraries. Counts were converted to $\log_2$ counts per million, then were quantile normalized and precision weighted with the voom function of the limma package[48]. A linear model was fitted to each gene[49], and empirical Bayes moderated *t*-statistics were used for analysis of differences in expression[50]. Genes were considered 'differentially expressed' if they achieved a false-discovery rate of 0.1 and an average RPKM value of ≥8 in at least one of the two groups being compared.

Histology. Colons were gently flushed clean and were cut into three sections corresponding to the proximal, middle and distal colon. Alternatively, colons were cut longitudinally and cleaned and then formed into a 'Swiss roll' for visualization of the full length of the colon after sectioning. The cecum was opened along the mesenteric side and its contents cleaned. Tissues were fixed in 10% neutral buffered formalin and were processed for wax embedding and routine staining with hematoxylin and eosin. The cecum was sectioned longitudinally, parallel to the mesenteric axis. Images were collected and analyzed with Aperio ImageScope v11.2.0.780 software. Colitis severity was assessed by researchers blinded to sample identity, by determining a combined score of infiltration of cells of the immune system and epithelial damage based on hyperproliferation, crypt loss and the presence of ulcers (**Supplementary Table 3**).

Colon homogenates. Explants of distal colon were isolated, weighed and cut. They were then homogenized in 2 ml of complete RPMI-1640 medium (as described above) and were incubated for 24 h at 37 °C. The supernatants were collected for cytokine measurement.

Cytokine measurement. IFN-γ, IL-17A, tumor-necrosis factor, IL-6, IL-1β, CXCL1 (KC) and IL-10 were assessed by cytometric bead array according to the manufacturer's protocol (BD Bioscience).

Microbiota sequencing. Fresh mouse stool samples were collected and were immediately stored at −80 °C. DNA was extracted from stools, and its quality and quantity were checked with a NanoDrop spectrophotometer and a Qubit fluorometer, together with the Broad Range assay (ThermoFisher). 'Barcoding' PCR was carried out with indexed primers targeting regions V3–V5 of the gene encoding 16S rRNA. AccuPrime Pfx SuperMix (12344-040; Invitrogen) was used for PCR. The PCR mix consisted of 18 µl of AccuPrime Pfx SuperMix, 0.5 µl of primers V3-340F and V5-926R (0.2 µM) and 1 µl of DNA (10 ng). PCR was carried out as follows: 95 °C for 2 min, 30 cycles of 95 °C for 20 s, 55 °C for 15 s and 72 °C for 5 min, and a final extension step at 72 °C for 10 min. PCR products were then quantified with the Qubit BR DNA assay kit. Equal amounts of each PCR mixture were pooled and thoroughly mixed. The amplicon pool was then loaded on an agarose gel (1.5%) and was separated by electrophoresis for 45 min at 100 V. The band corresponding to V3–V5 of the 16S rDNA amplicon was extracted from the gel and was purified with a Qiaquick gel-extraction kit (28704; Qiagen). Amplicon quantity and integrity were checked by electrophoresis through agarose gels and with the Qubit BR DNA assay kit. The amplicon was stored at −20 °C until use. The 16S rDNA amplicon library was sequenced at the Institut Curie NGS platform, on a MiSeq machine, with the 2 x 300 bp V3 kit (Illumina). Reads were merged with FLASH software ('fast length adjustment of short reads') and were trimmed with an in-house analysis script (length, ≥500 base pairs; quality, ≥25). Reads were clustered at 97% identity with the vsearch pipeline (https://zenodo.org/record/15524#Vky1U3t61ph). Chimeric operational taxonomic units (OTUs) were identified with the UCHIME algorithm and were discarded from subsequent analysis. The taxonomy of representative OTU sequences was determined with the RDP Classifier tool. OTU sequences were aligned by SSU-Align software. The phylogenetic tree was inferred from multiple alignments of the OTUs generated with the software Fattree2. Statistical analyses were performed with R software (R Development Core Team 2012) and various related packages (Ade4, Vegan, ape and phyloseq). Weighted UniFrac distances were calculated from a microbiota abundance table and phylogenetic tree. Statistical tests were performed with the Wilcoxon test (*P* value). The false-discovery rate method was used for correction for multiple testing (*q* value).

Quantification of segmented filamentous bacteria (SFB). Mice were housed by genotype, and feces were collected from mice at the age of 10 and 15 weeks. The protocol for DNA extraction was adapted from the published RBB+C method[51]. Feces were homogenized in lysis buffer with FASTprep (MP Biomedicals). DNA was precipitated in ammonium acetate and was washed with 70% ethanol. For the removal of RNA and protein, samples were further purified with a DNeasy Blood and Tissue Kit (Qiagen). Standard SYBRGreen quantitative PCR was performed. Detection of total bacteria was carried out with primers 1369f (5′-CGGTGAATACGTTCCCGG-3′) and 1492r (5′-TACGGCTACCTTGTTACGACTT-3′); SFB were detected with primers 779f (5′-TGTGGGTTGTGAATAACAAT-3′) and 1008r (5′-GCG GGCTTCCCTCATTACAAGG-3′). DNA from the feces of SFB single-colonized mice was used as a control for calculation of the relative amount of SFB by the Pfaffl method as follows: ratio = (E_target)^(ΔCT, target (calibrator–test))/(E_ref)^(ΔCT,ref (calibrator–test)).

Statistical analysis. All statistical analyses were performed with GraphPad Prism software, version 6.0d (Graphpad Software). We used an unpaired two-tailed Student's *t*-test for pairwise comparisons. An unpaired and paired Student's *t*-test, nonparametric Mann-Whitney test or Log-rank Mantel-Cox test was used for other comparisons.

42. Alonzi, T. *et al.* Essential role of STAT3 in the control of the acute-phase response as revealed by inducible gene inactivation [correction of activation] in the liver. *Mol. Cell. Biol.* **21**, 1621–1632 (2001).
43. Eberl, M., Jomaa, H. & Hayday, A.C. Integrated immune responses to infection - cross-talk between human γδ T cells and dendritic cells. *Immunology* **112**, 364–368 (2004).
44. Nieuwenhuis, E.E. *et al.* Disruption of T helper 2-immune responses in Epstein-Barr virus-induced gene 3-deficient mice. *Proc. Natl. Acad. Sci. USA* **99**, 16951–16956 (2002).
45. Narni-Mancinelli, E. *et al.* Fate mapping analysis of lymphoid cells expressing the NKp46 cell surface receptor. *Proc. Natl. Acad. Sci. USA* **108**, 18324–18329 (2011).
46. Thakur, C. *et al.* Increased expression of mdig predicts poorer survival of the breast cancer patients. *Gene* **535**, 218–224 (2014).
47. Liao, Y., Smyth, G.K. & Shi, W. featureCounts: an efficient general purpose program for assigning sequence reads to genomic features. *Bioinformatics* **30**, 923–930 (2014).
48. Ritchie, M.E. *et al.* limma powers differential expression analyses for RNA-sequencing and microarray studies. *Nucleic Acids Res.* **43**, e47 (2015).
49. Smyth, G.K. Linear models and empirical bayes methods for assessing differential expression in microarray experiments. *Stat. Appl. Genet. Mol. Biol.* **3**, 3 (2004).
50. McCarthy, D.J. & Smyth, G.K. Testing significance relative to a fold-change threshold is a TREAT. *Bioinformatics* **25**, 765–771 (2009).
51. Yu, Z. & Morrison, M. Improved extraction of PCR-quality community DNA from digesta and fecal samples. *Biotechniques* **36**, 808–812 (2004).

doi:10.1038/ni.3332